Application of generalized dispersion theory to vortex chromatography

Westerbeek, Eiko Y.; Gelin, Pierre; Frankel, Itzchak; Olthuis, Wouter; Eijkel, Jan C.T.; De Malsche, Wim

Published in:
Journal of Chromatography A

DOI:
10.1016/j.chroma.2022.462970

Publication date:
2022

Application of generalized dispersion theory to vortex chromatography

Eiko Y. Westerbeek[1,2], Pierre Gelin[1], Itzchak Frankel[3], Wouter Olthuis[2], Jan Eijkel[2], Wim De Malsche[1]

[1]µFlow group, Department of Chemical Engineering, Vrije Universiteit Brussel, Brussels, Belgium

[2] University of Twente. BIOS Lab on a Chip Group, MESA+ Institute for Nanotechnology & Max Planck Centre for Complex Fluid Dynamics, Enschede 7500 AE, the Netherlands

[3] Faculty of Aerospace Engineering, Technion-Israel Institute of Technology, Haifa 32000, Israel

Email corresponding author: wim.de.malsche@vub.be

Abstract

Acoustically induced secondary flows are applied to enhance lateral mass transfer beyond the relatively slow diffusion. This has the goal to reduce convective axial dispersion and the resulting band broadening which, in turn, limits the performance of column chromatography. Traditional approaches based on Taylor-Aris model are limited to one-dimensional rectilinear (unidirectional) tube- or channel-flows. We therefore apply the generalized dispersion theory (GDT) allowing for prediction of the dependence of potentially improved performance on the characteristics of the induced secondary flow, channel geometry and solute properties as well as providing qualitative physical insight into the role of lateral flows. Results corroborate agreement with our experimental observations (residual standard deviation, S_{res} = 3.88) and demonstrate the advantage of applying GDT relative to 3D time-dependent simulations.

Keywords: Generalized Dispersion Theory (GDT); Liquid chromatography; vortex; acoustofluidics

1. Introduction

The performance of a variety of continuous-flow systems such as liquid chromatography and continuous-flow chemistry is limited by axial dispersion resulting in broadening of sample bands. Ideally, it is desirable that the sample bands are transported as fast as possible to the detector downstream which favors relatively high carrier fluid speed, in order to minimize the analysis time. Under these conditions the primary contribution to axial dispersion is embodied in the C-term of van Deemter's relation, representing the effect of non-uniform axial (Poiseuille) fluid velocity (in pressure-driven flows) combined with the relatively slow diffusive solute transfer across streamlines. This mechanism was initially presented in the pioneering work of Taylor[1,2] and subsequently formally substantiated by Aris[3] via application of a statistical moments method.

A variety of methods to mitigate axial dispersion have been applied with only limited success. These include reduction of the dimensions of channel cross-section or modification of its shape[4][5] as well as passive mixing via Dean flow[6] or turbulent mixing. These however, are only effective at high axial velocities where dispersion is way too large to be relevant. Furthermore, passive mixing inevitably introduces undesirable axial-velocity components which enhance dispersion. Contrary to these passive approaches, active mixing[7–9] is applicable in a wide range of axial velocities while allowing for the generation of lateral flows accompanied by negligible axial-velocity components.

The goal of the present contribution is to investigate via both theoretical analysis and experimental methods the effectiveness of acoustically-induced lateral flows to the reduction of dispersion.

The above-mentioned Taylor[1,2] and Aris[3] analyses only considered solute transport in Poiseuille flow through a circular-cylindrical duct. Their results are therefore only applicable to one-dimensional rectilinear flows and as such do not allow for the analysis of the effect of the acoustically-induced lateral flow on solute dispersion. Effects of lateral flow have so far only been addressed theoretically[10,11]. In recent experimental work of our group we have actively induced a purely lateral flow leading to more uniform residence time and reduced dispersion. In [8] an oscillatory electric field perpendicular to channel axis and its top and bottom walls generates a time-averaged alternating current electroosmotic (ACEO) vertical lateral flow. In [9] such flow is acoustically excited in a channel (etched in silicon) connected to a piezoceramic element. Both methods enable the induction of nearly purely-lateral flow. These experiments demonstrated a reduction of the above-mentioned van Deemter's C-term by factors of 2 and 3, respectively. For the theoretical aspects, we here apply the generalized-dispersion-theory (GDT) paradigm introduced by Brenner[12,13]. This long-time asymptotic scheme (outlined in the following) provides in the present

context the effective transport coefficients, i.e. the axial velocity and dispersion coefficient in the presence of a generic lateral flow. We here apply GDT to examine the effects of the acoustically-induced lateral flow on dispersion. Results are compared to those obtained from full-scale simulations and band-broadening experimental data[9]. GDT also provides a valuable physical insight into the dispersion process. Since a reduction in dispersion gives a reduction in the plate height this also gives a prediction of the potentially-improved performance in open-tubular chromatography.

The rest of this contribution is organized as follows: We next describe the problem statement and then outline GDT. Subsequently, section 3 describes the simulations. We next discuss the results of the present model, in particular the effects of the lateral flow on the B-field essential to the rationalization of the reduction of axial dispersion. Results are then compared to those obtained via time-dependent 3D simulations and with experimental data respectively. Following the demonstrated agreement of the present analytic scheme with both simulations and experimental observations, GDT is applied to study the effects of channel cross-section dimensions and solute diffusivity on the potential reduction of dispersion via increased lateral flow. The paper ends with a conclusion and outlook.

2. Theory

2.1 Problem Statement within the framework of generalized dispersion theory

In the absence of irreversible chemical reactions, $c(x,y,z,t)$, the solute concentration distribution, satisfies the conservation convection-diffusion equation

$$\frac{\partial c}{\partial t} = u(x,y)\frac{\partial c}{\partial x} + v(x,y)\frac{\partial c}{\partial y} + U(x,y)\frac{\partial c}{\partial z} - D_m\nabla^2 c, \tag{1}$$

where $(x,y) \in S_0$, is the channel cross-section domain and $-\infty < z < \infty$ is the Cartesian coordinate along the straight open (modelled as infinitely-long-) channel , $\boldsymbol{u}(x,y) = \hat{\boldsymbol{\imath}}u + \hat{\boldsymbol{\jmath}}v$ is the lateral fluid velocity and $\widehat{\boldsymbol{k}}U(x,y)$ is the axial Poiseuille velocity, the constant D_m is the uniform isotropic molecular diffusivity of the solute and $\hat{\boldsymbol{\imath}}, \hat{\boldsymbol{\jmath}}$ and $\widehat{\boldsymbol{k}}$ are the unit vectors in x, y and z direction, respectively. The above conservation equation is supplemented with the boundary conditions

$$\boldsymbol{n}\cdot\boldsymbol{J} = \boldsymbol{n}\cdot(\boldsymbol{u}c - D_m\boldsymbol{\nabla}_\perp c) = 0\,, \tag{2}$$

with $\boldsymbol{n}$, the local unit vector normal to the boundary, $\boldsymbol{J}$ the solute cross-sectional flux and $\boldsymbol{\nabla}_\perp = \hat{\boldsymbol{\imath}}\frac{\partial}{\partial x} + \hat{\boldsymbol{\jmath}}\frac{\partial}{\partial y}$ the 'lateral' part of the gradient operation, thus representing impermeability of the channel walls to solute flux, the far-field condition

$$c(x,y,z,t) = 0, \qquad \text{as } |z| \to \infty \tag{3}$$

and the condition specifying $c(x,y,z,0)$, the initial solute-concentration distribution. In applications, the interest is primarily focused on the evolution of the cross-sectional averaged concentration

$$\bar{c}(z,t) = \frac{1}{|S_0|}\iint_{(x,y)\,\epsilon\,S_0} c(x,y,z,t)\,dxdy \tag{4}$$

rather than on the detailed information embodied in $c(x,y,z,t)$. This has been addressed for the specific problem of dispersion in Poiseuille flow within a circular cylindrical tube in the celebrated pioneering work of Taylor [1,2] and Aris [3] who established that, at times long relative to the cross-sectional diffusive relaxation time $\sim|S_0|/D_m$, $\bar{c}(z,t)$ satisfies the balance equation

$$\frac{\partial \bar{c}}{\partial t} + \frac{\partial \bar{J}}{\partial z} = 0, \tag{5a}$$

with the convection-diffusion constitutive relation for the solute mass flux

$$\bar{J} = \overline{U}\bar{c} - \overline{D}\frac{\partial \bar{c}}{\partial z}, \tag{5b}$$

where, similarly to Aris [3], the constant effective phenomenological coefficients are obtained from the long-time limits of the rate-of-change of the first-order and central second-order moments

$$\overline{U} = \frac{1}{M_0}\lim_{t\to\infty}\frac{dM_1}{dt} \tag{6a}$$

and

$$\overline{D} = \frac{1}{2M_0}\lim_{t\to\infty}\frac{d}{dt}(M_2 - M_1 M_1) \tag{6b}$$

of the first-order and central second-order moments

$$M_n = \int_{S_0}\int_{-\infty}^{\infty} z^n c(x,y,z,t)dz\ dxdy \quad for\ n = 0,1,\ldots \tag{6c}$$

In absence of chemical reactions, M_0 represents the conserved total amount of solute. The transport coefficients thus obtained represent the velocity along the channel of the solute center of mass and the rate of dispersion of the solute cloud. The actual evaluation of these is carried out within the framework of GDT as outlined in the next subsection. In van Deemter's theory, the linear mobile phase velocity is equal to $\overline{U}$ and the plate height is proportional to $\overline{D}$.

2.2 Generalized Dispersion Theory

The development by Brenner [10], [11] of GDT has been motivated by the recognition that certain fundamental elements of Taylor-Aris theory retain their validity and usefulness for a wide class of macrotransport problems well beyond the scope of their above-mentioned problem. Thus, GDT generalizes Aris' [3] moment scheme where their long-time asymptotic behavior provides the relevant macroscale description of the transport process. The generic problem is stated within an abstract multidimensional phase space consisting of the union of $\boldsymbol{q} \in \boldsymbol{q}_0$, a 'local', usually bounded, and a 'global' unbounded $\boldsymbol{Q} \in \boldsymbol{Q}_\infty$ subspaces while assuming all phenomenological coefficients to be exclusively dependent on the local coordinate $\boldsymbol{q}$. In the present problem the 'local' subspace $\boldsymbol{q}_0$ corresponds to the duct cross-sectional bounded domain $(x,y) \in S_0$and the 'global' domain is $\boldsymbol{Q}_\infty = z \in (-\infty,\infty)$, similarly to the classic Taylor-Aris problem.

The resulting GDT macro-transport paradigm [12] has allowed for the rigorous analysis of a broad class of material (e.g. dispersion of chemically-reactive and non-reactive solutes in continuous and discontinuous porous media, surface- and interfacial- transport, transport in physical space of solute particles possessing 'internal' orientation- or conformation degrees-of-freedom) as well non-material (dispersion of momentum and energy) problems. In the context of the present problem, application of GDT is essential to the study of the effect of the acoustically-induced lateral flow in view of the Taylor-Aris theory being strictly limited to one-dimensional unidirectional flows as noted above. Applied to the present problem GDT establishes that (at sufficiently long times) $\bar{c}(z,t)$, eq. (4), is governed by eqs. (5a,b) and (6) with the macro-scale transport coefficients constant and

128 independent of the initial state distribution, eq. (3). The macroscale velocity is obtained via the
129 integration over the duct cross-section

130 $$\overline{U} = \frac{1}{M_0}\int_{(x,y)\in S_0} c_0(x,y)U(x,y)\ dxdy \tag{7a}$$

131 where the stationary field c_0 is in the long-time limit

132 $$c_0(x,y) = \lim_{t\to\infty}\int_{-\infty}^{\infty} c(x,y,z,t)dz\,. \tag{7b}$$

133

134 Normalizing solute concentration by the (conserved) total amount of solute, c_0 thus defined
135 represents the fraction of solute along the straight line parallel to the z-axis and passing through
136 (x,y). It is governed by the 'local'-subspace boundary-value problem

137 $$\boldsymbol{\nabla}_\perp\cdot(\boldsymbol{u}c_0 - D_m\boldsymbol{\nabla}_\perp c_0) = 0\,, \tag{8a}$$

138 together with the boundary-

139 $$\hat{\boldsymbol{n}}\cdot(\boldsymbol{u}c - D_m\boldsymbol{\nabla}_\perp c) = 0 \tag{8b}$$

140 and normalization-

141 $$\int_{S_0} c_0 dxdy = 1 \tag{8c}$$

142 conditions. In the absence of external force fields, solute is passively convected in the ambient
143 incompressible flow field satisfying $\boldsymbol{\nabla}_\perp\cdot\boldsymbol{u} = 0$ and $\hat{\boldsymbol{n}}\cdot\boldsymbol{u} = 0$, i.e. impermeability of the duct wall to
144 the fluid, c_0 is uniform across S_0, the duct cross-section. Thus $c_0 = 1/|S_0|$ where $|S_0|$ denotes the
145 cross-sectional area. The effective solute velocity $\overline{U}$ is thus equal to the cross-sectional average of the
146 carrier fluid axial velocity. The effective macroscale dispersivity is $\overline{D} = \overline{D}_m + \overline{D}_c$ thus including the
147 contributions of molecular diffusion

148 $$\overline{D}_m = \int_{S_0} c_0 D_m dxdy = D_m \tag{9a}$$

149 in view of the uniformity of c_0, and the Taylor-dispersion coefficient

150 $$\overline{D}_c = \frac{1}{|S_0|}\int_{S_0} B(x,y)[U(x,y) - \overline{U}]dxdy, \tag{9b}$$

151 respectively, where the $B(x,y)$ field is defined by the long-time limit

152 $$B(x,y) = \lim_{t\to\infty}\{\frac{1}{c_0}\int_{S_0} zc(x,y,z,t)dz - \overline{U}t\}. \tag{10}$$

153 Similarly to the above c_0, the asymptotic analysis establishes that $B(x,y)$ thus defined is indeed
154 stationary and independent of the initial solute distribution $c(x,y,z,0)$. The first term on the RHS of
155 eq. (10) represents the time variation of center-of-mass of the fraction of solute along the straight
156 line parallel to the z-axis passing through the point (x,y) within the duct cross-section S_0. The
157 kinematic significance of eq. (10) is that $B(x,y)$ represents in the long-time limit the *constant* axial
158 distance between solute centroid along each of these axial lines and the center of mass of the entire
159 solute cloud, respectively. The B-field is effectively obtained from the boundary-value problem

$$\nabla_\perp \cdot (\boldsymbol{u}(x,y)B - D_m \nabla_\perp B) = U(x,y) - \overline{U} \tag{11a}$$

within S_0 together with the condition

$$\boldsymbol{n} \cdot (\boldsymbol{u}B - D_m \nabla_\perp B) = 0 \tag{11b}$$

on the boundaries of the duct cross-section. These determine B to within an arbitrary additive constant $\overline{B}$ which, in turn, as can be verified readily from the definition of $\overline{U}$ (eq. 7a), has no effect on $\overline{D}_c$ (eq. 9b). We thus render $B(x,y)$ unique by imposing the additional normalization condition

$$\int_{S_0} B(x,y)dxdy = 0 \tag{11c}$$

In summary, for $U(x,y)$, $\boldsymbol{u}(x,y)$ and D_m given, the fields $c_0(x,y)$ and $B(x,y)$ are obtainable from eqs. (8a-c) and (11a-c), respectively. The effective macroscale transport coefficient $\overline{U}$ and $\overline{D}$ appearing in the constitutive equation of the axial solute flux (eq. 5b) are then evaluated from eqs. (7a),(9a) and (9b).

3. Method

Computations were performed on a HP workstation running Windows 10 Enterprise (64-bits) equipped with 32 GB RAM and a hexacore Intel processor (I7-4930K), using COMSOL Multiphysics (version 5.3). First, dispersion was determined based on three-dimensional time-dependent simulations wherein a solute plug was injected and followed through time. Depending on the applied velocities, these simulations took up to 12 hours. The results thus obtained were compared with dispersion coefficients obtained with the generalized dispersion theory.

3.1 Time dependent model

The band broadening simulations were performed in an open rectangular channel with dimensions of 37.5 µm x 15.0 µm x 5.0 mm (Fig. 1). This geometry was meshed using 2 625 152 cells, with an average mesh quality of 0.67. A Poiseuille flow was applied in the axial direction and acoustic streaming in the lateral direction. The velocity field of the acoustic streaming was determined using the limiting velocity method (LVM) described by Lei *et al.* [14]. As this method only solves the outer boundary streaming with the assumption of an incompressible flow and neglectable inertial terms and thermoviscous effects, the computation time is minimized. Using the module 'Transport of Diluted Species' a solute plug (D_m=5.4x10^{-10} m^2/s) was injected at t=0. The integral over the cross section, $\int c(x,y,z,t)dA$, at two axial positions (4 mm and 5 mm downstream) was determined and used to evaluate the axial dispersion coefficient and the reduced plate height $h = \frac{\Delta\sigma_z^2}{\Delta z} \cdot \frac{1}{l}$ with σ_z the standard deviation of the solute distribution in the axial direction and l the characteristic length, being the height of the channel.

3.2 GDT implementation

For the implementation of GDT, COMSOL was used to determine the different solutions.

Axial flow

Since most chromatographic systems are pressure driven, we use an axial pressure-driven flow in this work. The Hagen–Poiseuille equation was used to determine the flow in axial direction through the cross-section of the channel

$$\frac{\partial^2 v}{\partial y^2} + \frac{\partial^2 u}{\partial x^2} = -\frac{G}{\mu} \tag{12a}$$

where $G = \frac{dp}{dz}$, μ the viscosity of the fluid and the boundary conditions are

$$u(x,0) = u(x,h) = 0 \quad (12b)$$
$$u(0,y) = u(w,y) = 0 \quad (12c)$$

197

198 While there exists a semi-analytic solution[15] we found it more convenient for our present purpose
199 to use the numerical solution. The cross sectional geometry was meshed using 31 768 cells with an
200 average mesh quality of 0.94.

201 ### Lateral flow

202 Boundary-driven acoustic streaming is a flow phenomenon induced at the channel walls and allows for
203 the generation of long-range (10^{-3} m) lateral flows with a negligible axial component. Furthermore,
204 acoustic streaming has been well studied from both a theoretical and experimental point of view [16–
205 19]. To induce acoustic streaming, a microchannel is usually placed on a piezoceramic element which
206 operates at the resonance frequency of the fluid-filled microfluidic channel. To achieve resonance the
207 channel width (w) should be a multiple of half the wavelength λ (w = n*λ/2). For submillimeter
208 channels filled with water, the resonance frequency is within the low MHz range. Similar to the 3D
209 simulations, the LVM method was used to determine the lateral velocity field.

210 ## 4. Results & Discussion

211 In the employed acoustic streaming system, the axial flow is a conventional Poiseuille flow (see Fig.
212 2a). In Fig. 2 b, the lateral, acoustically induced, flow profile as obtained by CFD is depicted, showing
213 the occurrence of 4 main vortices characteristic for half wavelength actuation (w = λ/2).

214 The magnitude of the vortices depends on the channel dimensions and amplitude of wall
215 displacement. Using Eqs. 11a – 11c, the B-field (Fig. 2c) is uniquely determined. As stated in section
216 2, the B-field can be given a kinematic interpretation as the distance between the axial center of mass
217 of the entire solute slug and the axial center of mass of the slug at a specific coordinate in the cross-
218 section.

219 By eq. (9b), when seeking to minimize dispersion for a given pressure-driven (Poiseuille) channel flow
220 and solute-carrier-fluid pair, it is desirable to modify the distribution of $B(x,y)$ through the
221 introduction of a secondary (lateral) flow $u(x,y)$ (cf. 11a). Figure 3 presents the evolution of the
222 $B(x,y)$ field with increasing lateral Péclet number, $Pe_{lat} = |\boldsymbol{u}|_{av}h/D_m$,where $|\boldsymbol{u}|_{av}$ denotes the
223 average lateral fluid speed over the channel cross-section and h is the channel depth.

224 By the double mirror-image symmetry of both $u(x,y)$ and $B(x,y)$ (figure 2b and 2c, respectively), in
225 figure 3 we only present the lower-right quarter of the channel cross-section. The various subfigures
226 present the level lines of $B(x,y)$ together with corresponding distributions of the relative
227 magnitudes, of $B(x,y)$, across the domain. It is important to note that, as mentioned above, the
228 colour code is not uniform, but rather specific to each part of the figure. The caption of the figure
229 details the range of values in each part. With increasing Pe_{lat} we note that the level line pattern is
230 becoming similar to the corresponding streamline pattern of the secondary flow (cf. figure 2b and
231 2c). Indeed, by the dimensionless version of eq (11a), with increasing Pe_{lat} >>1 for a fixed value of
232 $Pe_{ax} = \overline{U}h/D_m$, the equation reduces to:

233 $$\boldsymbol{u} \cdot \boldsymbol{\nabla} B = 0 \quad (11a')$$

234 The above implies that the value of *B* is constant along each streamline of the lateral flow. It is,
235 however important to note that owing to the singularity of the limit $Pe >> 1$, the effect of the weak
236 diffusion is non-negligible. It typically occurs in transport problems, characterized by the occurrence
237 of closed streamlines or particle trajectories, that [20–22] the (weak) diffusion affects the relatively

slow transport across streamlines or particle trajectories. This determines the long-time limit (relevant to Taylor dispersion) distribution of B between the level lines (with remains indeterminate otherwise). As can be observed in figure 3, the lateral acoustically-driven flow, acts to diminish the range of the B-values, i.e. uniformize $B(x, y)$ which, in turn corresponds to diminishing B which is in agreement with the kinematic significance of $B(x, y)$. From equation 9b follows that when diminishing $B(x, y)$, the dispersion also diminishes.

4.1 Comparison with time-dependent numerical model

We compared a full-scale 3D-time dependent numerical simulation with our GDT-model and both have been compared to a semi-analytical model proposed by Poppe [23] (the latter in absence of secondary flow). As can be observed from Fig. 4, in which the plate height is plotted against the axial velocity, both models are in good agreement with the semi-analytical model. A residual standard deviation (S_{res}) has been calculated for both models which gave 0.0564 and 0.0467, respectively. The agreement between the different models can be observed from Fig. 4, in which the plate height is plotted against the axial velocity.

The results of the time-dependent simulation model and the generalized dispersion theory are in good agreement with each other at all lateral and axial velocities simulated (S_{res} = 0.0622). The former, however, took several hours to run, while the latter approximation is obtained within a minute. Although the generalized dispersion theory is in principle only valid in the long time-limit, good agreement between the results of both models is already achieved for relatively short channels (typically within axial distances comparable to 10 times the channel depth downstream from where the solute plug is introduced). This suggests that GDT can be used to determine the dispersion for most experimentally relevant channel lengths. Another benefit of applying the generalized dispersion theory to dispersion problems is the physical insight into the problem in terms of the B-field distribution and its variation resulting from lateral convection.

4.2 Comparison with experimental results.

To assess the validity and usefulness of the application of the GDT in an experimental setting, a comparison with, earlier published[9], experimental data has been performed as well. The dispersion experiments were performed in silicon chips with a channel of dimensions 375 µm x 33 µm (w x h). The chip was connected to a piezo-ceramic element (15 x 20 x 1 mm, APC International Lt., USA) and actuated at a frequency of 1.95Mhz (Fig 1b.). The actuator was driven by a frequency generator (AFG Tektronix UK Ltd., UK) and the voltage was amplified by a RF power amplifier (210L, Electronics & Innovation, USA). The medium inside the channel was DI water and the injected plug was DI water containing the fluorescent dye, Fluorescein isothiocyanate (FITC). The reduced plate height was determined by injecting a plug of FITC into a microchannel in the presence of acoustically induced lateral flow and subsequent measurement of its width at the point of injection and 5mm downstream. The measured lateral velocity was used as a fitting parameter for the simulation of the acoustofluidic model. The lateral velocity field thus simulated has, in turn, been used as an input for the generalized dispersion model.

Figure 5 presents the effect of induced secondary flow on the variation of reduced plate height with Pe_{ax} representing the reduced axial velocity. Squares and circles represent experimental values and theoretical (GDT) predictions, respectively. The red symbols represent the variation in the absence of lateral flow, blue symbols correspond to $Pe_{lat} = 47$. In both cases there is a good agreement between corresponding experimental observation and theoretical (GDT) predictions. Both show a reduction of plate height by a factor of 2 as a result of the induced lateral flow. To reduce the plate height, most

efforts in the last decades have been devoted to reducing the characteristic length of the system. In packed bed columns this is done by reducing the particle size and in open-tubular columns this is done by reducing the dimensions of the cross-section of the channel. Furthermore, the A-term in the van Deemter equation has been reduced by using open-tubular columns or by using ordered pillar arrays[24,25]. Reducing the C-term by inducing lateral convection, is a totally new approach in the field of chromatography and figure 5 shows that a substantial reduction can be made using this. A next step would be to make an open-tubular column with porous walls in which convection can be induced.

4.3 Variation of dispersion coefficient for different dimensions and diffusivity coefficient of the solute

In silicon chip chromatography as well as in acoustofluidic applications, microchannels are often rectangular with aspect ratios being unequal to one. The variation of dispersion in microchannels of varying aspect ratios is well documented in the absence of lateral flow [4,23]. Furthermore the dispersion in microchannels of various shapes, packed with porous particles has been studied theoretically[26] as well as experimentally[27]. Here, we turn to consider the effect of increasing lateral acoustofluidic flow on the dispersion coefficient in rectangular microchannels with varying cross-sectional aspect ratio AR and solute molecular diffusivity. To this end, Fig. 6 presents the variation with Pe_{lat}/Pe_{ax} of $\overline{D}_c/\overline{D}_{c0}$ for rectangular microchannels of uniform width (375 μm) and several combinations of depth to width aspect ratio AR, and solute diffusion coefficients D_m, (AR, D_m) = (2.5, $10^{-10}\ m/s^2$, red), (11, $10^{-10}\ m/s^2$, blue) and (11, 5.4x$10^{-10}\ m/s^2$, yellow).

We see that increasing either AR or D_m results in a less significant relative reduction of the dispersion coefficient. These trends reflect the fact that the secondary flow is only affecting $\overline{D}_c$, the convective 'Taylor' part of $\overline{D}$, while, with increasing either AR or D_m, the relative contribution of $\overline{D}_c$ is decreasing. This reduction in $\overline{D}_c$ results in a lower contribution from the van Deemter's C-term and therefor to lower plate heights.

To further reduce the dispersion coefficient for given AR and diffusion coefficient, one could in principle seek the most optimal lateral flow pattern. In practice however, the lower bounds will most often not be reached and therefore focusing on inducing a high lateral velocity will be a more effective strategy in reducing dispersion.

To evaluate the potential gain of the vortex chromatography method for the best possible conditions for performing analytical separations, it is interesting to examine how downscaling of the channel size affects the dispersion coefficient. In Fig. 7, a channel of 375 μm x 150 μm is successively scaled down, first by a factor of 10 and then by a factor of 100 at a fixed axial velocity in the C-term regime and forD_m = 10^{-10} m^2/s and D_m = 10^{-12} m^2/s, respectively corresponding to relatively small and large analyte molecules. Similar to Fig. 6, in all cases presented the relative dispersion coefficient decreases monotonically decreasing with increasing Pe_{lat}/Pe_{ax}. As observed in Fig. 3, with enhanced secondary flow the B field approaches uniformity throughout the channel cross section, which results in diminishing $\overline{D}_c$, the 'convective' Taylor term accompanied by the dispersion coefficient approaching the lower limit, i.e. the solute molecular diffusivity $\overline{D} \rightarrow \overline{D}_m$. What can be appreciated from figures 6 and 7 is that the major portion of the potential reduction of $\overline{D}$ is already achieved at relatively small ratio of lateral- to axial- fluid velocities. This is particularly visible for the combination of larger cross-sectional dimensions and smaller solute diffusivity, i.e. those cases where the convective effect

represented by $\overline{D}_c$, the Taylor term, is significant. From Fig. 7 it is clear that for all cases, at a relative streaming velocity $Pe_{lat}/Pe_{ax} = 0.5$, a reduction of dispersion by a factor of 10 or larger is generally attained. At values of $Pe_{lat}/Pe_{ax} = 2$, even a gain of close to 2 orders of magnitude is predicted.

5. Conclusion & Outlook

In this work we describe the application of the generalized dispersion theory to demonstrate the effective reduction of Taylor dispersion and show that it is in good agreement with the experimental results for dispersion in microchannels. We showed furthermore that using GDT is far less computational power demanding than a 3D time-dependent simulation.

We discussed the usability of lateral mixing with acoustic streaming for microchannels with different sizes and aspect ratios. However, currently available acoustic actuators put a lower limit to the channel size. Currently available PZT frequencies are in the range of 20 MHz, limiting one of the channel dimensions to 37.5 µm. Current research, however, aims at integrating films of PZT material into the microfluidic channels, allowing for actuation frequencies higher than 100 MHz [28,29]. At a frequency of 100 MHz, channel sizes of 7.5 µm can be used with water as a mobile phase. For the electroosmotic approach however, the smallest dimension in which vortices can be produced is sub-micron, which might therefore be an approach that can be more readily put in practice. We also showed that the average lateral flow speed needs to be sufficiently high to induce sufficient gain. Experimental work is underway aiming at lateral flows in the hundreds of µm/s in such micron-scale channels.

The present study has not considered the potential effects of solute retention/ adsorption. Because of an increasing C-term contribution to dispersion at increasing retention, it is expected that lateral flows will result in a significant dispersion reduction under retained conditions. This aspect will be at the focus of a follow-up study. Future work can also study how different types of lateral flows can be used to reduce Taylor-Aris dispersion. Thus, while the present model has only considered steady lateral flows, future work will examine the potential effects of time-periodic lateral flows.

6. Acknowledgements

WDM, PG and EW greatly acknowledge the European Research Council for the support through the ERC Starting Grant EVODIS (grant number 679033EVODIS ERC-2015-STG) and the MMICAS project (HBC.2020.2627) supported by VLAIO/Catalisti

References

[1] G. Taylor, Dispersion of soluble matter in solvent flowing slowly through a tube, Proc. R. Soc. London. Ser. A. Math. Phys. Sci. 219 (1953) 186–203. https://doi.org/10.1098/rspa.1953.0139.

[2] G.I. Taylor, Diffusion and mass transport in tubes, Proc. Phys. Soc. Sect. B. 67 (1954) 857–869. https://doi.org/10.1088/0370-1301/67/12/301.

[3] R. Aris, On the dispersion of a solute in a fluid flowing through a tube, Proc. R. Soc. London A. 235 (1956) 67–77. https://doi.org/10.1098/rspa.1956.0065.

[4] M. Callewaert, W. De Malsche, H. Ottevaere, H. Thienpont, G. Desmet, Assessment and numerical search for minimal taylor-aris dispersion in micro-machined channels of nearly rectangular cross-section, J. Chromatogr. A. 1368 (2014) 70–81. https://doi.org/10.1016/j.chroma.2014.09.009.

[5] G. Lee, A. Luner, J. Marzuola, D.M. Harris, Dispersion control in pressure-driven flow through bowed rectangular microchannels, Microfluid. Nanofluidics. 25 (2021) 1–11.

https://doi.org/10.1007/s10404-021-02436-9.

[6] A. Lewandrowska, A. Majcher, A. Ochab-Marcinek, M. Tabaka, R. Hołyst, Taylor dispersion analysis in coiled capillaries at high flow rates, Anal. Chem. 85 (2013) 4051–4056. https://doi.org/10.1021/ac4007792.

[7] P. Hajiani, F. Larachi, Reducing Taylor dispersion in capillary laminar flows using magnetically excited nanoparticles: Nanomixing mechanism for micro/nanoscale applications, Chem. Eng. J. 203 (2012) 492–498. https://doi.org/10.1016/j.cej.2012.05.030.

[8] E.Y. Westerbeek, J.G. Bomer, W. Olthuis, J.C.T. Eijkel, W. De Malsche, Reduction of Taylor-Aris dispersion by lateral mixing for chromatographic applications, Lab Chip. 20 (2020) 3938–3947. https://doi.org/10.1039/d0lc00773k.

[9] P. Gelin, D. Maes, W. De Malsche, Reducing Taylor-Aris dispersion by exploiting lateral convection associated with acoustic streaming, Chem. Eng. J. (2020) 128031. https://doi.org/10.1016/j.cej.2020.128031.

[10] H. Zhao, H.H. Bau, Effect of secondary flows on Taylor-Aris dispersion, Anal. Chem. 79 (2007) 7792–7798. https://doi.org/10.1021/ac701681b.

[11] A. Adrover, Effect of secondary flows on dispersion in finite-length channels at high Peclet numbers, Phys. Fluids. 25 (2013). https://doi.org/10.1063/1.4820214.

[12] H. Brenner, A general theory of Taylor dispersion phenomena, Physicochem. Hydrodyn. 1 (1980) 91–123.

[13] H. Brenner, A general theory of Taylor dispersion phenomena. II An extension, Physicochem. Hydrodyn. 3 (1982) 139–157.

[14] J. Lei, P. Glynne-Jones, M. Hill, Comparing methods for the modelling of boundary-driven streaming in acoustofluidic devices, Microfluid. Nanofluidics. 21 (2017) 1–11. https://doi.org/10.1007/s10404-017-1865-z.

[15] H. Bruus, Theoretical microfluidics, 2008.

[16] P. Gelin, Ö. Sardan Sukas, K. Hellemans, D. Maes, W. De Malsche, Study on the mixing and migration behavior of micron-size particles in acoustofluidics, Chem. Eng. J. 369 (2019) 370–375. https://doi.org/10.1016/j.cej.2019.03.004.

[17] P.B. Muller, H. Bruus, Theoretical study of time-dependent, ultrasound-induced acoustic streaming in microchannels, Phys. Rev. E - Stat. Nonlinear, Soft Matter Phys. 92 (2015) 1–13. https://doi.org/10.1103/PhysRevE.92.063018.

[18] R. Barnkob, P. Augustsson, T. Laurell, H. Bruus, Acoustic radiation- and streaming-induced microparticle velocities determined by microparticle image velocimetry in an ultrasound symmetry plane, Phys. Rev. E - Stat. Nonlinear, Soft Matter Phys. 86 (2012). https://doi.org/10.1103/PhysRevE.86.056307.

[19] P.B. Muller, M. Rossi, A.G. Marín, R. Barnkob, P. Augustsson, T. Laurell, C.J. Kähler, H. Bruus, Ultrasound-induced acoustophoretic motion of microparticles in three dimensions, Phys. Rev. E - Stat. Nonlinear, Soft Matter Phys. 88 (2013) 1–12. https://doi.org/10.1103/PhysRevE.88.023006.

[20] L.G. Leal, E.J. Hinch, The effect of weak Brownian rotations on particles in shear flow, J. Fluid Mech. 46 (1971) 685–703. https://doi.org/10.1017/S0022112071000788.

[21] E.J. Hinch, L.G. Leal, The effect of Brownian motion on the rheological properties of a

suspension of non-spherical particles, J. Fluid Mech. 52 (1972) 683–712. https://doi.org/10.1017/S002211207200271X.

[22] G.K. Batchelor, On steady laminar flow with closed streamlines at large Reynolds number, J. Fluid Mech. 1 (1956) 177–190. https://doi.org/10.1017/S0022112056000123.

[23] H. Poppe, Mass transfer in rectangular chromatographic channels, J. Chromatogr. A. 948 (2002) 3–17. https://doi.org/10.1016/S0021-9673(01)01372-3.

[24] X. Illa, W. De Malsche, J. Bomer, H. Gardeniers, J. Eijkel, J.R. Morante, A. Romano-Rodríguez, G. Desmet, An array of ordered pillars with retentive properties for pressure-driven liquid chromatography fabricated directly from an unmodified cyclo olefin polymer, Lab Chip. 9 (2009) 1511–1516. https://doi.org/10.1039/b818918h.

[25] W. De Malsche, D. Clicq, V. Verdoold, P. Gzil, G. Desmet, H. Gardeniers, Integration of porous layers in ordered pillar arrays for liquid chromatography, Lab Chip. 7 (2007) 1705–1711. https://doi.org/10.1039/b710507j.

[26] S. Khirevich, A. Höltzel, D. Hlushkou, A. Seidel-Morgenstern, U. Tallarek, Structure-transport analysis for particulate packings in trapezoidal microchip separation channels, Lab Chip. 8 (2008) 1801–1808. https://doi.org/10.1039/b810688f.

[27] S. Jung, A. Höltzel, S. Ehlert, J.A. Mora, K. Kraiczek, M. Dittmann, G.P. Rozing, U. Tallarek, Impact of conduit geometry on the performance of typical particulate microchip packings, Anal. Chem. 81 (2009) 10193–10200. https://doi.org/10.1021/ac902069x.

[28] P. Reichert, D. Deshmukh, L. Lebovitz, J. Dual, Thin film piezoelectrics for bulk acoustic wave (BAW) acoustophoresis, Lab Chip. 18 (2018) 3655–3667. https://doi.org/10.1039/c8lc00833g.

[29] Y.Q. Fu, J.K. Luo, N.T. Nguyen, A.J. Walton, A.J. Flewitt, X.T. Zu, Y. Li, G. McHale, A. Matthews, E. Iborra, H. Du, W.I. Milne, Advances in piezoelectric thin films for acoustic biosensors, acoustofluidics and lab-on-chip applications, Prog. Mater. Sci. 89 (2017) 31–91. https://doi.org/10.1016/j.pmatsci.2017.04.006.

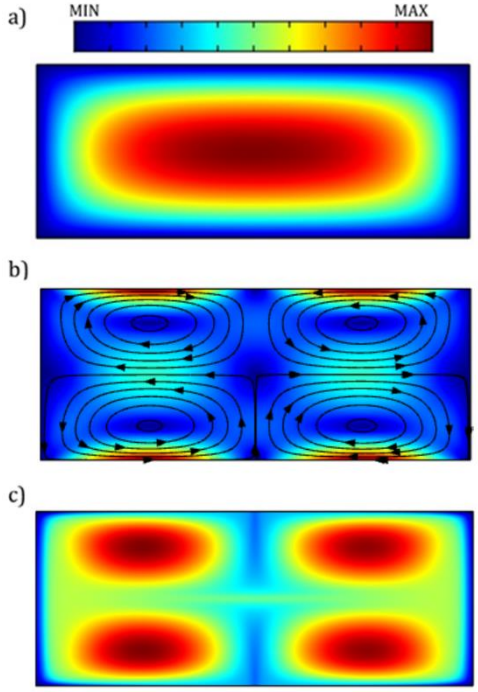

437

438 **Figure 1:** The relevant fields appearing in the model: a) axial velocity field, b) lateral velocity field and c) B-field
439 The colour code indicates the relative magnitudes of axial- (a) and lateral- (b) fluid speeds and (c) B-field
440 distribution.

441

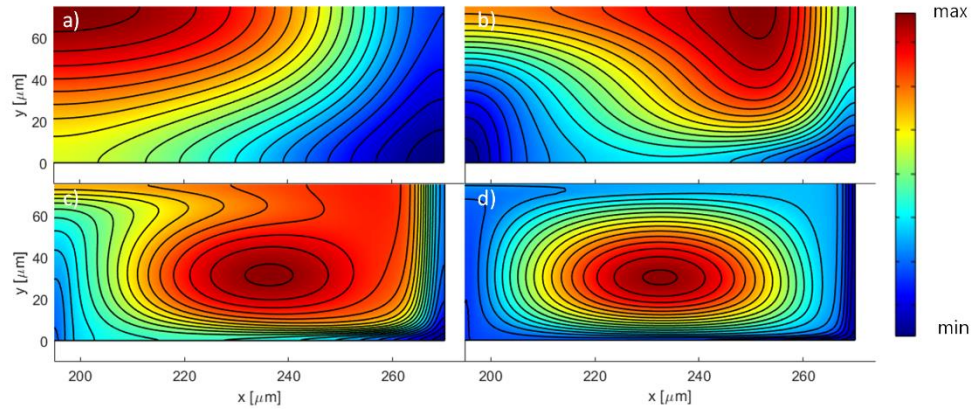

442

443 **Figure 2:** level lines of the B-field distribution in the bottom-right quarter of the duct cross section for $Pe_{ax} =$
444 783 and Pe_{lat} : a) 3, b) 30, c) 300 and d) 3000. The level lines show constant values of the B-field, the color
445 shows the B-field distribution, with as maximum and minimum value, a) 6200 μm, -6572 μm b) 1179 μm, -
446 1429 μm c) 205.8 μm , -406.1 μm d) 193.4 μm, -175.4 μm.

447

448

449

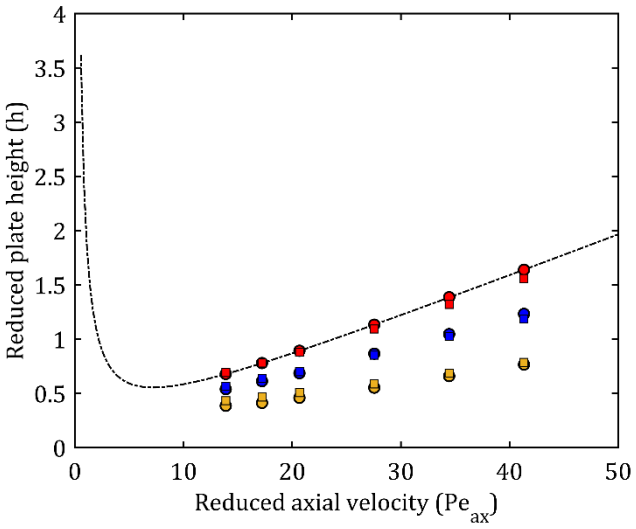

Figure 3: Effect of acoustic streaming on the reduced plate height as a function of reduced axial velocity for a channel with a cross-section of dimensions 37.5 x 15 µm. 3D Time dependent simulations (circles) as well as simulations applying the Generalized Dispersion Theory (squares) were performed, with the average lateral speeds, Pe_{lat} being 0(red), 15 (blue) and 30 (yellow).

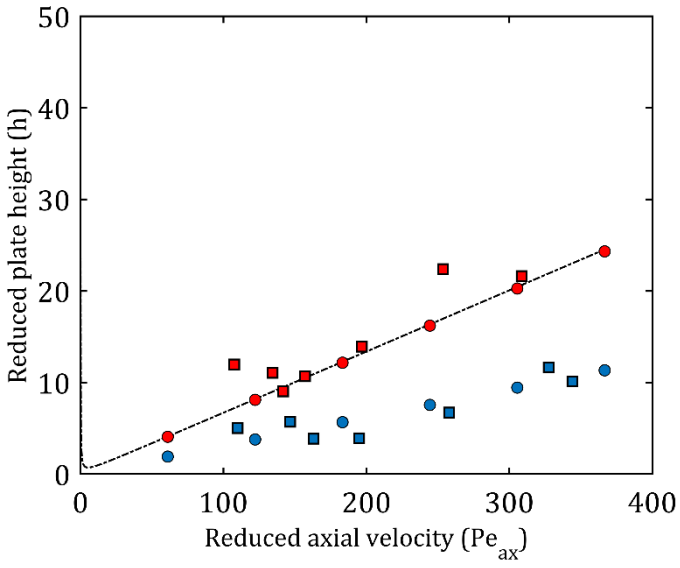

Figure 4: Comparison of simulations performed with GDT and experimental data obtained for channels with a rectangular cross section of 375 x 33 µm. The theoretical curve (dotted line) is obtained from a semi-analytic expression for the plate height without lateral flow [22]. Squares display experimental values, circles display values obtained with GDT. Red denotes results obtained in the absence of lateral flow and blue denotes results obtained with an average lateral Péclet number of 5.5.

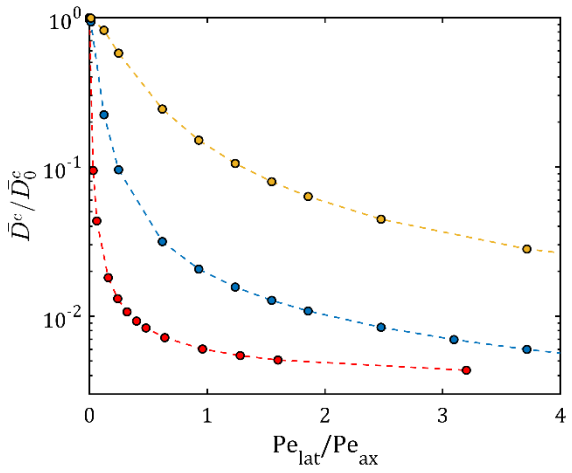

Figure 5: Effects of aspect ratio (AR) and diffusion coefficient (D^m) on the relative Taylor-Ais dispersion coefficient as a function of velocity ratios of the average lateral and average axial speed. For channel width=375 µm and depths depending on the aspect ratio and average axial Péclet number of 78. Indicated by red, AR=2,5 and $D^m = 1 * 10^{-10}$, blue, AR=11 and $D^m = 1 * 10^{-10}$ and yellow, AR=11 and $D^m = 5.4 * 10^{-10}$.

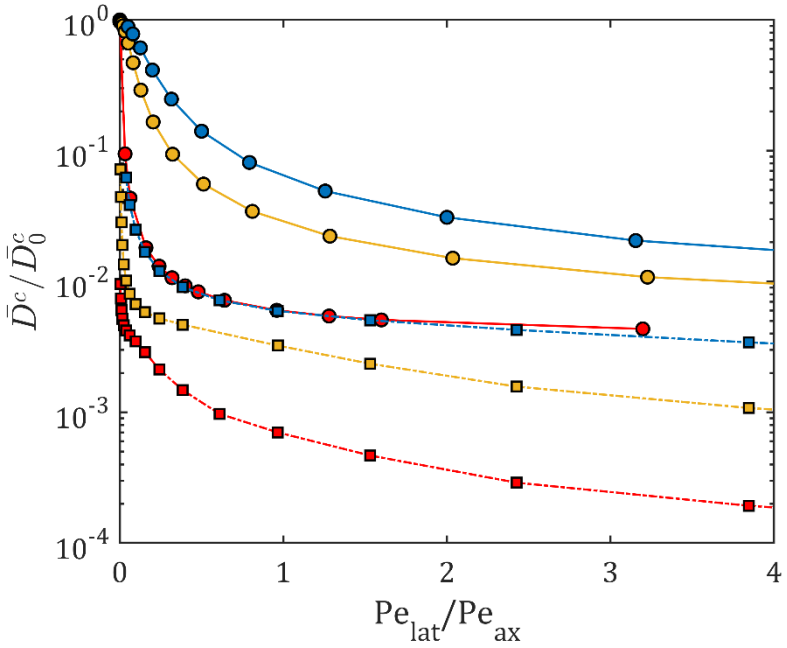

Figure 6: Effects of solute diffusion coefficient and downscaling of channel cross-section dimensions on the variation of the relative Taylor-Aris dispersion coefficient with the ratio of average lateral- and axial- speed. The axial velocity is fixed well into the C-term regime. Red circles, 375x150 µm, $D^m = 1 * 10^{-10}$. Yellow circles, 37.5x15 µm, $D^m = 1 * 10^{-10}$. Blue circles, 3.75x1.5 µm, $D^m = 1 * 10^{-10}$. Red squares, 375x150 µm, $D^m = 1 * 10^{-12}$. Yellow squares, 37.5x15.0 µm, $D^m = 1 * 10^{-12}$. Blue squares, 3.75x1.50 µm, $D^m = 1 * 10^{-12}$